Journal of Applied Physics

RESEARCH ARTICLE | JUNE 24 2026

Investigation of the environmental influence on C(V) characteristics of gallium nitride metal–insulator–semiconductor high-electron-mobility transistors

Special Collection: Frontiers in Nitride Semiconductors Research

B. Weber ✉ ; M. Dammann; P. Brückner ; P. Straňák ; L. Kirste ; H. Czap; M. Baeumler ; H. Konstanzer; P. Neininger; P. Merkert ; R. Quay

Check for updates

J. Appl. Phys. 139, 245703 (2026)
https://doi.org/10.1063/5.0325135

View Online
Export Citation

Articles You May Be Interested In

Negative-bias temperature instability in AlSiO/p-type GaN metal-oxide-semiconductor field-effect transistors with ultrathin AlN interfacial layer

J. Appl. Phys. (June 2026)

Ion polarization behavior in alumina under pulsed gate bias stress

Appl. Phys. Lett. (March 2015)

Electrical characteristics of tungsten-doped InZnSnO thin film transistors by RF magnetron sputtering

J. Vac. Sci. Technol. B (March 2022)

13 July 2026 05:29:28

Zurich Instruments
Freedom to Innovate.
The New VHFLI 200 MHz Lock-in Amplifier.
Orchestrate pulses, triggers, and acquisition as the hub of your experiment.
Discover more – run every signal analysis tool, simultaneously.
Order now

AIP Publishing

Journal of Applied Physics ARTICLE pubs.aip.org/aip/jap

Investigation of the environmental influence on C(V) characteristics of gallium nitride metal–insulator–semiconductor high-electron-mobility transistors

Cite as: J. Appl. Phys. **139**, 245703 (2026); doi: 10.1063/5.0325135
Submitted: 29 January 2026 · Accepted: 4 June 2026 ·
Published Online: 24 June 2026

View Online Export Citation CrossMark

B. Weber,[a] M. Dammann, P. Brückner, P. Straňák, L. Kirste, H. Czap, M. Baeumler, H. Konstanzer, P. Neininger, P. Merkert, and R. Quay

AFFILIATIONS

Fraunhofer Institute for Applied Solid State Physics (IAF), Tullastr, 72, 79108 Freiburg, Germany

Note: This paper is part of the Special Topic on Frontiers in Nitride Semiconductors Research.
[a]**Author to whom correspondence should be addressed:** benjamin.weber@iaf.fraunhofer.de

ABSTRACT

This study examines the impact of humidity and temperature on the reliability of silicon nitride (SiN) passivated 80 μm gallium nitride (GaN) metal–insulator–semiconductor high-electron mobility transistor (HEMT) test structures. Degradation is determined by threshold voltage shifts in the capacitance–voltage C(V) characteristics. High temperature and humidity, while maintaining a constant gate and drain bias, are deleterious to reliability, leading to pronounced positive threshold voltage shifts (ΔV_{th}). In contrast to previous humidity studies on Schottky-gate GaN HEMTs, which reported negligible humidity-induced threshold shifts, the present work shows that GaN MISHEMTs exhibit a strong sensitivity of ΔV_{th} to humidity. A lifetime analysis based on Peck's model was conducted to quantify these effects, yielding a humidity acceleration factor $B = 0.021$ at 85 °C and an activation energy $E_a = 0.45$ eV in ambient air. It has been shown that increasing the relative humidity (RH) from 0% to 40% reduces the time to failure by approximately one order of magnitude. A comparison of different SiN passivation thicknesses reveals that thick gate passivation substantially mitigates humidity-induced degradation. Time-of-flight secondary ion mass spectrometry (ToF-SIMS) analysis showed that degradation mainly occurs in the access region rather than the intrinsic region. The presence of oxidized SiN passivation and cracks was revealed by both ToF-SIMS and scanning electron microscopy/element-dispersive x-ray analysis of these regions. The epitaxial layers and the SiN passivation are identical to those of short-channel (100 nm) GaN HEMTs, meaning that these findings can be transferred.

© 2026 Author(s). All article content, except where otherwise noted, is licensed under a Creative Commons Attribution (CC BY) license (https://creativecommons.org/licenses/by/4.0/). https://doi.org/10.1063/5.0325135

I. INTRODUCTION

Gallium nitride (GaN) technology enables higher power and frequencies, making it suitable for diverse applications in fields such as consumer electronics, aerospace, and defense. GaN is ideal for these applications because its wide bandgap and high electron mobility enable efficient operation at high voltages, high frequencies, and high temperatures, resulting in smaller, lighter, and more energy-efficient systems.[1] The latter two categories require particularly reliable performance under harsh conditions. It has previously been demonstrated that both temperature[2–4] and humidity[5,6] have a detrimental effect on the lifespan of GaN high-electron mobility transistors (HEMTs). Most of these studies have focused on Schottky-gate HEMTs and have evaluated degradation primarily by means of dc or RF figures of merit, such as drain current, threshold voltage, and on-resistance, under off-state or on-state stress.[2,7–10] Systematic investigations of GaN MISHEMTs, which incorporate a gate dielectric and SiN passivation stack and therefore introduce additional, moisture-sensitive interfaces, are still limited. GaN MISHEMTs exhibit high current drive and low gate leakage, which render them suitable for high-voltage and high-power

13 July 2026 05:29:28

© Author(s) 2026

applications.[11,12] However, this device type is still suffering from reliability issues that impede its commercial application.[13,14] Nitride-based gate dielectrics are an interesting subject of research for GaN metal–insulator–semiconductor high-electron mobility transistor (HEMT) test structures (MISHEMT TS), given their ability to inhibit or prevent the formation of Ga–O bonds.[15]

To date, the combined influence of humidity and temperature on GaN MISHEMTs with SiN-based passivation has not been systematically quantified.

In particular, (i) the acceleration of C(V)-derived ΔV_{th}-shifts under controlled humidity and temperature in HTRB/H^3TRB conditions, (ii) the role of SiN passivation thickness and gate passivation configuration in mitigating humidity-induced degradation, and (iii) the localization of degradation within the access region as opposed to the intrinsic region have not been comprehensively clarified for GaN MISHEMTs. Moreover, humidity-accelerated degradation has rarely been captured for these devices within a unified lifetime framework such as Peck's model, and the extracted model parameters have not been directly correlated with microscopic failure mechanisms in the MIS gate stack.

The present study addresses these gaps by evaluating the C(V) characteristics of simple GaN MISHEMT TS under the stressors of humidity and temperature in HTRB/H^3TRB stress tests. Section 2 provides a detailed exposition of the technology employed and the measurement conditions. In Sec. III, the experimental results are described and interpreted: ΔV_{th}-shifts extracted from C(V) are used as the primary degradation metric to evaluate the reliability and derive the TTF. A lifetime analysis is performed to obtain a humidity acceleration factor B and an activation energy E_a, which are combined in Peck's model to describe the environmental acceleration of degradation. Furthermore, the influence of SiN passivation thickness is examined by comparing different MISHEMT TS, and a detailed failure analysis based on time-of-flight secondary ion mass spectrometry (ToF-SIMS) and scanning electron microscopy/element-dispersive x-ray (SEM/EDX) analysis is carried out to localize and identify the dominant degradation mechanisms (Secs. III and IV). The objective of Sec. V is to provide a concise overview of the key findings from the preceding sections.

II. TECHNOLOGY AND MEASUREMENTS

In this work, two MISHEMT TS are compared, which are based on corresponding HEMT structures. The processing of the corresponding HEMTs is described for TS1[16,17] and TS2[18,19] in detail in the literature. This section will focus on the differences between these technologies and their implications for reliability. Both TS are displayed in Fig. 1. TS1 incorporates a thin AlN interlayer. It is assumed that this enhances the charge carrier density in the 2DEG[20] and improves the electron confinement in the GaN channel.[21,22] Additionally, this process enhances electron mobility.[23] The enhanced charge carrier density enables higher output power, while the higher mobilities facilitate RF applications. Ohmic contacts are composed of Ti/Al, and TiPtAu is utilized as the gate metal. Furthermore, the ohmic contacts are enhanced by Si ion implantation to reduce the contact resistance. After Si implantation, a high-temperature anneal is required to activate the

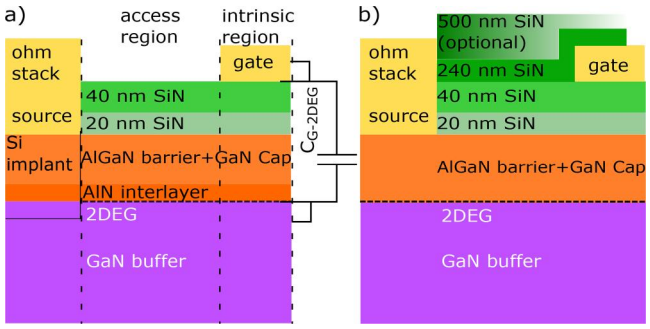

FIG. 1. Cross-sectional schematics of two different GaN MISHEMT TS with varying SiN passivation layers. (a) TS 1 has a thin SiN passivation, an AlN interlayer, and ohmic contacts are enhanced by Si ion implantation. (b) TS 2 has additional gate passivation.

Si ions. This process has the potential to cause diffusion and degradation of the epitaxy, which may consequently have a detrimental effect on reliability. TS1 employs a very thin SiN passivation layer. TS2 is distinguished by the absence of an AlGaN interlayer and ohmic contact implantation. In contrast, TS2 exhibits an additional gate SiN passivation.

The reliability assessment of the GaN MISHEMTs is based on changes in their capacitance–voltage C(V) characteristics. C(V) measurements determine the depletion voltage between the gate metal and the 2DEG (contacted by the ohmic contact), which is based on a parallel plate capacitor.[24] Figure 2 illustrates a capacitance–voltage C(V) and conductance–voltage G(V) curve for the GaN MISHEMT TS1 at 100 kHz. In the region below the threshold voltage, the channel is depleted (low capacitance) and begins

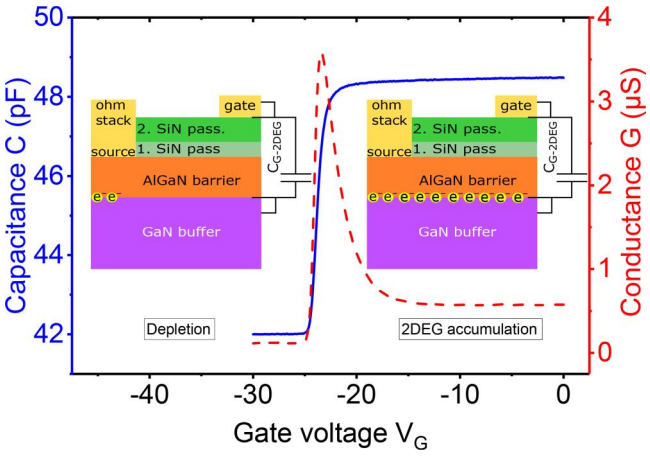

FIG. 2. Capacitance–voltage C(V) and conductance–voltage G(V) characteristics of an AlGaN/GaN MISHEMT structure. The left schematic illustrates the depletion region, where the two-dimensional electron gas (2DEG) is absent. As the voltage increases beyond the threshold voltage (V_{th}), 2DEG accumulation occurs, as shown in the right schematic.

13 July 2026 05:29:28

© Author(s) 2026

to accumulate as the voltage increases. This is accompanied by a sharp increase in the conductance. V_{th} is determined at the sharp rise in the C(V) curve at the mid-capacity between the upper and lower plateau.[25] The combination of the sharp rise in capacitance with the aforementioned factors indicates a high-quality interface between the semiconductor and the insulator.[26] The upper plateau of the capacitance is denoted as C_{tot}.

The average threshold voltage shift ΔV_{th} of two devices per test conditions is the principal metric employed to evaluate the degradation of the device. The GaN MISHEMTs feature a gate length of 80 μm and a width of 100 μm, mounted in commercial packages with silver-filled adhesive. Unless stated otherwise, TS1 was used for all reliability tests and failure analysis.

A. ToF-SIMS

The chemical composition of the GaN MISHEMTs was analyzed using the M6 Plus (IONTOF GmbH) ToF-SIMS instrument through depth profiling in dual beam mode. A 1 keV Cs^+ sputter ion beam, operating at an ion beam current of approximately 10 nA, was used together with a 30 keV Bi^+ primary ion beam for crater analysis at 0.05 pA, all incident at an angle of 45°. The sputter ion beam was rastered over an area of $250 \times 250\ \mu m^2$, while the primary beam was focused on a smaller $130 \times 130\ \mu m^2$ raster area at the center of the crater to minimize crater edge effects while still covering the entire device area. The region of interest (ROI) can be selected specifically after the measurement.

Under these imaging conditions, the lateral resolution is limited by the pixel size rather than the primary ion beam. For an image size of 256×256 pixels over the selected raster area, the corresponding pixel size is approximately 0.51 μm, which represents the effective lateral resolution. The instrument operated under ultra-high vacuum (UHV) conditions at a pressure of 3×10^{-10} mbar. The measurements were conducted with the detector in negative polarity, and an electron flood gun was used to decrease the charging effects.

B. SEM/EDX

Scanning electron microscopy (SEM) was performed using a Zeiss Auriga 40 system equipped with an Orsay Physics focused ion beam (FIB) column and a Bruker energy-dispersive x-ray spectroscopy (EDX) detector. SEM images were acquired at an accelerating voltage of 10 kV and a working distance of 5 mm.

III. RELIABILITY RESULTS

First, the experiments involved the variation in humidity levels and temperature, and the results of which are presented here. The threshold voltage shift has been employed in prior literature as a failure criterion.[27–29] To determine a time to failure (TTF) for the GaN MISHEMT TS, the failure criterion $\Delta V_{th} > 2$ V was set. The underlying Peck model is explained in more detail in Sec. III C.

A. Influence of humidity

The presence of moisture can accelerate the process of degradation through a phenomenon known as moisture-assisted charge trapping,[30,31] which, in turn, leads to dielectric weakening and shifts of threshold voltage.[32] The penetration of moisture has been demonstrated to induce the formation of hydroxyl groups at the dielectric/semiconductor interface.[6] This has been shown to increase interface state density and to promote defect generation.

To achieve a more profound comprehension of the impact of humidity-induced degradation in the on-state condition, an investigation into the impact of humidity levels ranging from 0% to 85% was conducted under elevated temperatures and forward bias conditions (HTRB, $V_G = -20$ V; $V_D = 10$ V) at a baseplate temperature of $T_{bp} = 85$ °C. The incorporation of humidity in this test design results in its designation as the H^3TRB test. The H^3TRB test is a well-established method of reliability testing that utilizes high humidity, elevated temperatures, and a high reverse bias.[30,33,34] The results for the GaN MISHEMT TS1 are presented in Fig. 3.

Following a duration of 70 h, samples exposed to the most severe conditions (85% relative humidity and 85 °C) demonstrated the fastest degradation, exhibiting a ΔV_{th}-shift greater than 20 V. At 40% relative humidity, a comparable ΔV_{th}-shift occurred after 200 h, whereas at 20% relative humidity, the shift was observed after exceeding 1000 h. The presence of low humidity conditions [corresponding to approximately 3% relative humidity (RH) in air and 0% RH in nitrogen] resulted in ΔV_{th}-shift of 2–3 V, with devices exposed to nitrogen exhibiting marginally smaller shifts in comparison to those exposed to ambient conditions.

For an RH of 40%, the on-resistance R_{on} has been measured and is shown in Fig. 4. Even before 100 h, there is an immense increase in R_{on} of over 100%. The cause of this increase is discussed in Sec. IV.

In comparison to the presented data, it is noteworthy that Gao *et al.*[6] did not observe ΔV_{th} in GaN HEMTs under off-state conditions with high humidity. Consequently, it can be deduced

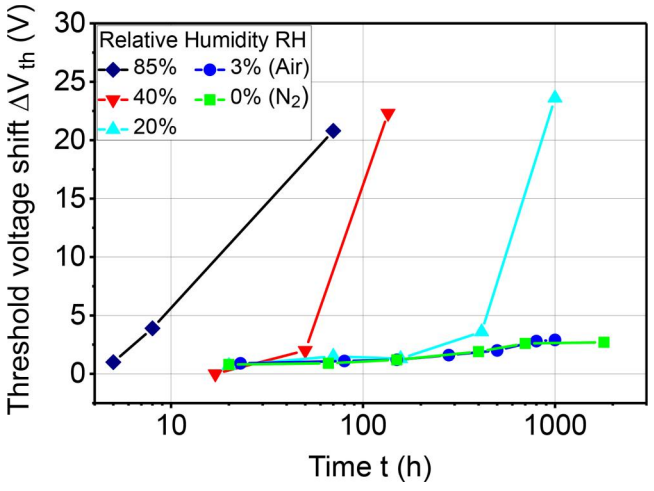

FIG. 3. Average ($n = 2$ devices) threshold voltage shift (ΔV_{th} in V) over stress time (t in h) during on-state test ($V_G = -20$ V; $V_D = 10$ V) with varying relative humidity (RH) at 85 °C. Elevated humidity levels significantly accelerate degradation, with the fastest degradation at 85% RH.

13 July 2026 05:29:28

© Author(s) 2026

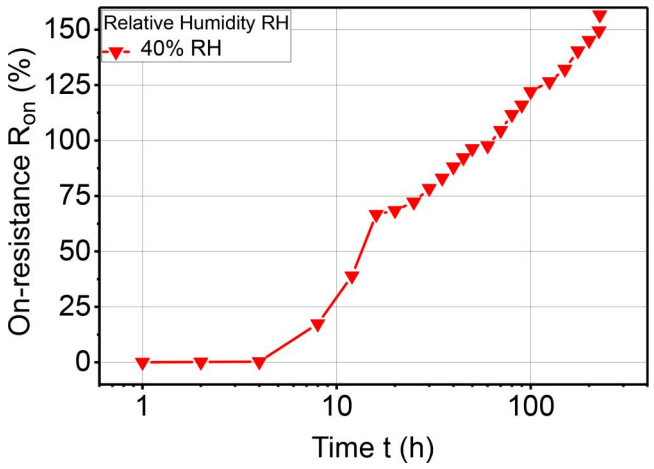

FIG. 4. Average ($n = 2$ devices) on-resistance (R_{on} in %) over stress time (t in h) during HTRB ($V_G = -20$ V; $V_D = 10$ V) with 40% RH at 85 °C. The influence of humidity significantly increases R_{on}.

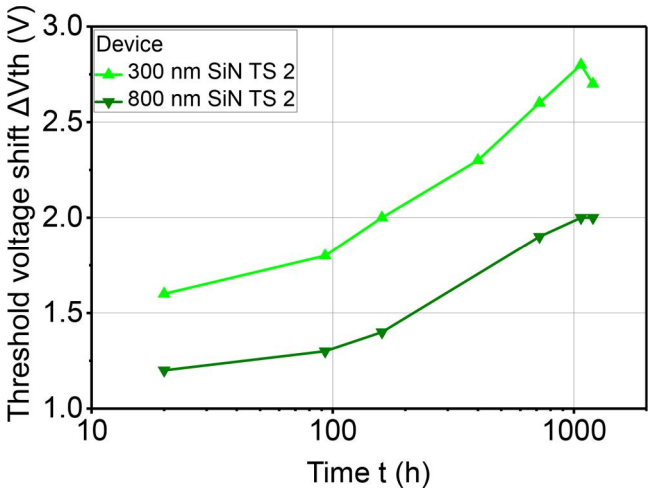

FIG. 5. Average ($n = 2$ devices) threshold voltage shift (ΔV_{th} in V) over stress time (t in h) during on-state ($V_G = -20$ V; $V_D = 10$ V) at 85% relative humidity (RH) and 85 °C. It illustrates the V_{th}-behavior for various SiN passivation thicknesses.

that these GaN HEMTs exhibit a reduced susceptibility to moisture-induced threshold voltage shifts in comparison to GaN MISHEMTs. Similarly to this work, for GaAs p-HEMTs, it was observed that ΔV_{th} was in positive direction under humid conditions. The value of V_{th} is contingent upon the orientation of the gate. The piezoelectric effect is the determining factor, given that the stress in proximity to the gate is subject to alteration.[35] A similar correlation was identified in the context of GaN power amplifiers (PA), whereby an increase in humidity resulted in a decline in performance, as evidenced by a reduction in PAE and output power.[36]

The deleterious impact of humidity on device performance can also be proved by comparing devices with different passivation thickness (TS2). The results are displayed in Fig. 5. TS2 with 300 nm SiN passivation displayed a V_{th}-shift of 2.7 V after 1000 h, whereas TS2 with 800 nm SiN passivation has an even lower V_{th}-shift of 2.0 V. It can thus be concluded that the additional gate passivation compared to TS1 (V_{th}-shift of 20 V after 70 h) significantly reduces the humidity-induced degradation, thereby underlining the tremendous effect of high humidity and the effectiveness of thick SiN gate passivation.

However, it has to be noted that TS1 and TS2 have different epitaxy and processing (see Fig. 1). Therefore, only the two TS2 with different passivation thicknesses can be compared directly. The comparison to TS1 could potentially indicate that thinner passivation leads to faster degradation.

Overall, the detrimental effect of ΔV_{th} shifts can be mitigated by the application of a thick SiN passivation layer, which is an effective means of blocking humidity.

B. Influence of temperature

Temperature is a critical factor in the degradation behavior of GaN MISHEMTs, given that many of the underlying physical mechanisms like charge trapping/detrapping,[32,37,38] dielectric breakdown,[11,39] defect generation,[40] and water/hydrogen diffusion[41] are thermally activated. The analysis of the temperature dependence of the TTF provides insights into the dominant degradation mechanisms and their associated activation energies. It is widely acknowledged that material properties and device behavior exhibit a strong temperature dependence. The aforementioned effects alter the electron mobility,[4] saturation velocity,[42] and the thermomechanical stress arising from the differences between the coefficient of thermal expansion (CTE) of the different materials.[43] To gain a more profound understanding of the impact of temperature-accelerated degradation in the on-state condition, a baseplate temperature range T_{bp} from 100 to 200 °C was systematically investigated under forward bias ($V_G = -20$ V; $V_D = 10$ V) conditions in ambient air atmosphere.

The results for TS1 are presented in Fig. 6. It can be deduced that the devices at 200 °C and 175 °C undergo rapid degradation, reaching the failure criterion before 100 h.

Devices at 150 and 100 °C demonstrate substantially reduced degradation rates, reaching the failure criterion between 100 and 200 h and between 300 and 400 h, respectively. As the operating temperature of the device increases from 100 to 200 °C, there is a gradual decline in lifetime.

C. Combined lifetime analysis

A significant number of thermally activated degradation mechanisms demonstrate a temperature dependence that adheres to the Arrhenius law as mentioned in Sec. III B. In order to account for the influence of humidity, an additional term is added, resulting in the formulation of Peck's model. The Peck model[44] is a widely used empirical reliability model that describes

13 July 2026 05:29:28

© Author(s) 2026

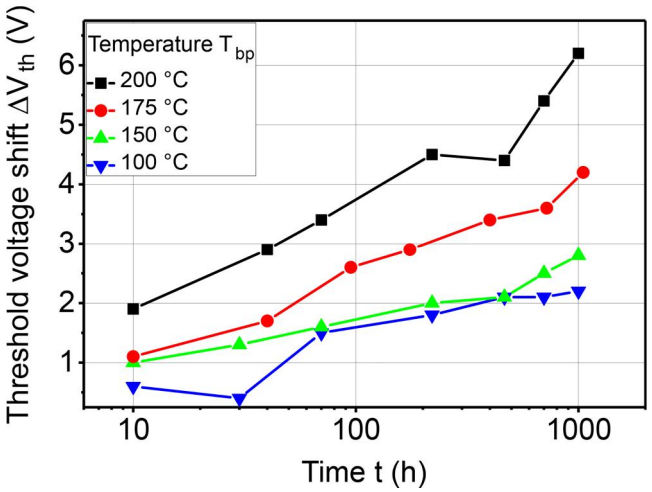

FIG. 6. Average ($n = 2$ devices) threshold voltage shift (ΔV_{th} in V) over stress time (t in h) during HTRB ($V_G = -20$ V; $V_D = 10$ V) with varying temperature in ambient air atmosphere. Higher base plate temperatures T_{bp} significantly accelerate degradation.

how humidity and temperature accelerate degradation processes, particularly in semiconductor devices and electronics. It is particularly useful in accelerated life testing under harsh environmental conditions.[44]

It is described in logarithmic version in Eq. (1),

$$\log_{10}(\mathrm{TTF}) = -B \cdot \mathrm{RH} - \frac{E_a}{\ln(10) \cdot k_B \cdot T} + C. \quad (1)$$

In Eq. (1), TTF denotes the time to failure, which decreases with increasing relative humidity (RH) and temperature (T). The parameter B is the humidity acceleration factor, representing the sensitivity of degradation to moisture. The activation energy E_a reflects the thermal activation barrier of the dominant failure mechanism, while k_B is Boltzmann's constant. The constant C captures baseline effects, including pre-exponential terms and intrinsic material properties not directly influenced by humidity or temperature. The parameters for humidity (B) at 85 °C and temperature (E_a) in air are extracted and interpreted separately in Fig. 7(a) and 7(b), respectively.

The linear fit of Fig. 7(a) for TS1, including the parameters, is given in Eq. (2),

$$\log_{10}(TTF) = -0.021 \cdot RH + 2.591. \quad (2)$$

It has been found that increasing the humidity from 0% to 40% reduces the TTF by one order of magnitude. This shows that humidity significantly affects the rate of degradation and contributes to the overall deterioration of the material. The systematic investigation of humidity and extraction of B for GaN MISHEMTs has not been performed in the literature yet.

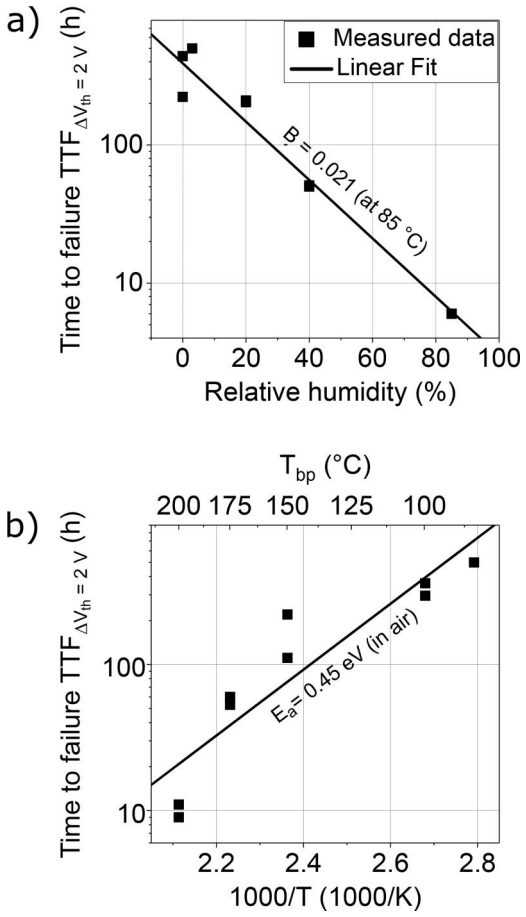

FIG. 7. Logarithmic time to failure (TTF) plotted against the (a) relative humidity (RH) and (b) temperature, respectively. The acquired data were fitted with a linear function (parameters are shown in the graph).

The linear fit of Fig. 7(b) for the GaN MISHEMT TS, including the parameters, is given in Eq. (3),

$$\log_{10}(\mathrm{TTF}) = -\frac{0.45}{k_B \cdot T \cdot \ln(10)} - 3.07. \quad (3)$$

The extracted activation energy is 0.45 eV. The study by Meneghini *et al.*[28] determined an activation energy of 0.37 eV for GaN MISHEMTs, suggesting that trapping is the primary degradation process.

However, those devices exhibit a significantly smaller gate length of 0.6 μm compared to 80 μm in this work.

The ensuing formulation of Peck's model for GaN MISHEMT TS is arrived at through the combination of both parameters, namely, B and E_a,

$$\log_{10}(\mathrm{TTF}) = -0.021 \cdot \mathrm{RH} - \frac{0.45}{\ln(10) \cdot k_B \cdot T} + C. \quad (4)$$

13 July 2026 05:29:28

© Author(s) 2026

Moisture sensitivity and activation energy can facilitate the determination of the degradation mechanism. Section IV undertakes a thorough failure analysis to gain a more profound understanding of the underlying degradation mechanism.

IV. FAILURE ANALYSIS

To gain a more profound comprehension of the factors that give rise to device failure, a systematic investigation is employed on selected stressed TS1 devices (along with a reference device). The process entails the probing of their morphology, element distribution, and depth profiling. The former can be accomplished through the utilization of SEM and EDX mappings, while the latter is attainable by ToF-SIMS. ToF-SIMS can also be utilized to probe the element distribution, a method offering considerably higher detection sensitivity than SEM-EDX. Conversely, SEM-EDX offers higher spatial resolution. Evidently, the degradation rate is significantly influenced by the humidity levels in the environment and temperature. It can be hypothesized that the accumulation of oxygen at specific interfaces serves as a potential explanation for this observed degradation mechanism, although further research in this area is required. To facilitate better comprehension, a light microscope (LM) overview image is presented, which shows the unstressed [Fig. 8(a)] and stressed devices [Fig. 8(b)]. As can be seen, the device under test (DUT) has three contact points: source (S), gate (G), and drain (D). The same labelling is used for the SEM and EDX images, and the device orientation is identical. The substantial degradation of the device on both the source and the drain side is already apparent in the light microscope image, as indicated in Fig. 8(b). Figure 8 shows which areas are investigated in greater detail by means of SIMS and SEM/EDX.

The I(V) and C(V) characteristics of the stressed device are shown in Fig. 9.

The device exhibits a strong threshold voltage shift of $\Delta V_{th} = 20$ V after 70 h in the C(V) curve. At 70 h, there is also a second transition in the C(V) curve visible, which can be attributed to the barrier accumulation besides the main transition, which can be attributed to the 2DEG accumulation.[25] The same shift can be observed in the I(V) curve as well.

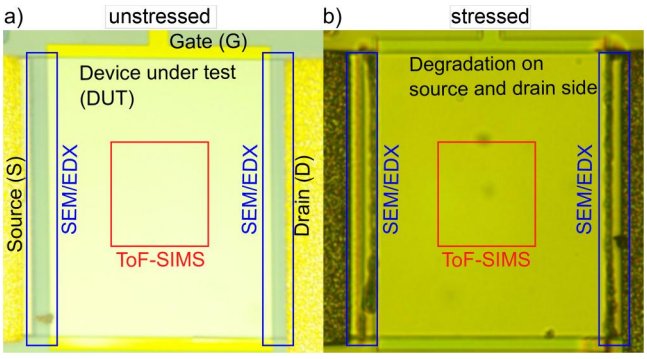

FIG. 8. Light microscope (LM) image of the unstressed (a) and stressed (b) devices. The overview image shows the source (S), gate (G), and drain (D) contacts of the device under test (DUT). It also indicates which areas have been investigated by SIMS and SEM/EDX analysis. The ToF-SIMS region of interest (ROI) was 31 × 31 μm^2.

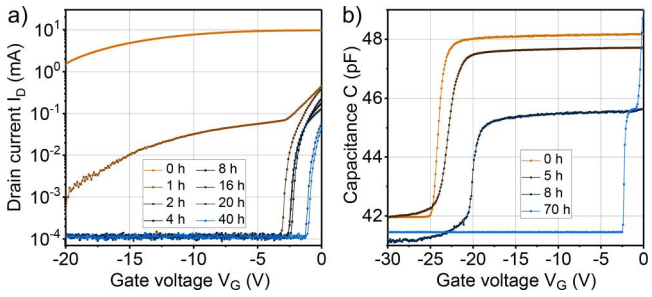

FIG. 9. (a) I(V) and (b) C(V) transfer characteristics of the stressed device (85% relative humidity (RH); base plate temperature $T_{bp} = 85$ °C; gate voltage $V_G = -20$ V; drain voltage $V_D = 10$ V; stress time $t_{stress} = 70$ h). The DUT is a TS 1 with a gate length $l_G = 80\,\mu$m. Both curves demonstrate the strong $\Delta V_{th} = 20$ V.

A. Depth profiling and element distribution by ToF-SIMS

Initially, a comprehensive investigation was undertaken, encompassing an extensive area within the gate metal of both an unstressed and a stressed device. This investigation was facilitated by the ToF-SIMS technique, with the primary objective being to discern any potential disparities that might have been caused by stressing the aforementioned device. The ToF-SIMS depth profiles, displayed in Fig. 10, demonstrate the SiN^- and GaN^- signal for both devices. The peaks of oxygen and hydroxyl (*OH*) groups are located at the SiN/gate metal interface and at the semiconductor/SiN interface, indicating a greater accumulation of oxygen at these interfaces. It is noteworthy that the O^- and OH^- ion counts of the stressed and unstressed devices match. This finding indicates that the oxygen present is of an intrinsic nature, arising as a consequence of the processing rather than from the high humidity. The region beneath the gate metal (intrinsic region) was found to be protected by the gate metal itself. However, analysis of the LM images of Fig. 8 indicates that degradation of the gate metal in the access region is evident at the edges. To highlight the differences between the smaller areas in the access region and the intrinsic regions [see Fig. 1(a)] of the unstressed and stressed devices, ToF-SIMS depth profiling was used to investigate these areas. First, a comparison of the ToF-SIMS depth profiles of the access and intrinsic region of the unstressed device is shown in Fig. 11.

The shapes of $AlGaN^-$, SiN^-, and O in the access region 2 and the intrinsic region 1 are analogous, even though the latter is considerably broader. It is apparent that, to reach the intrinsic region 1, it is necessary to first sputter through the 570 nm-thick gate metal, which has been omitted from the profile. The ion beam does not remove atomic layers in a layer-by-layer manner. Consequently, atoms from adjacent layers have the potential to mix. This phenomenon results in less sharp interfaces and a

13 July 2026 05:29:28

© Author(s) 2026

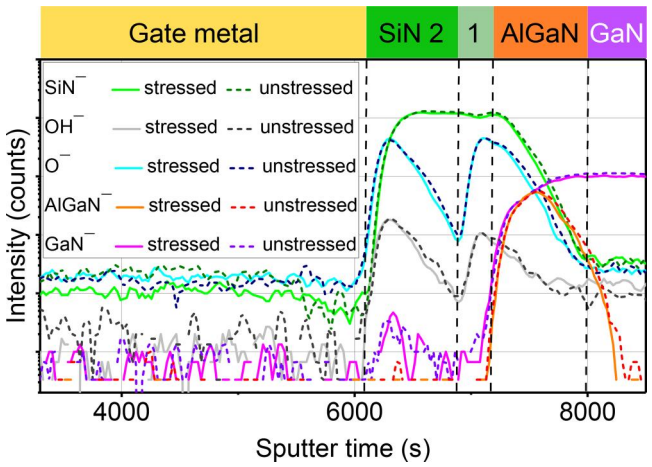

FIG. 10. ToF-SIMS profiles of a large area through the gate metal (intrinsic region) of an unstressed and a stressed device (85% relative humidity (RH); base plate temperature $T_{bp} = 85\,°C$; gate voltage $V_G = -20\,V$; drain voltage $V_D = 10\,V$; stress time $t_{stress} = 70\,h$). The ToF-SIMS ROI was $31 \times 31\,\mu m^2$. No differences in signal intensities could be detected between the unstressed and stressed device.

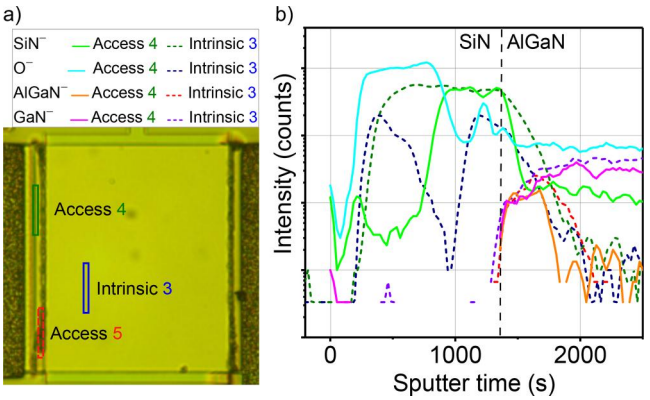

FIG. 12. (a) Locations of ToF-SIMS profiles of small areas in the intrinsic region 3 and the access region 4 of a stressed device [85% relative humidity (RH); base plate temperature $T_{bp} = 85\,°C$; gate voltage $V_G = -20\,V$; drain voltage $V_D = 10\,V$; stress time $t_{stress} = 70\,h$]; (b) corresponding ToF-SIMS profiles to 3 and 4. ToF-SIMS profiles of access region 5 have been measured but could not be evaluated due to too strong degradation. The ToF-SIMS region of interest was $1.5 \times 28\,\mu m^2$. Overall, the access region exhibits significantly higher oxygen levels throughout the SiN passivation and the AlGaN/GaN epitaxial layers.

broadening of the signal, which is also observable in this instance.[45] The oxygen signal exhibits a marginally elevated intensity in the access region; however, this is justifiable given that this surface is exposed to the ambient atmosphere, as opposed to being covered by the gate metal. Second, the comparison is repeated for a stressed device, as illustrated in Fig. 12. The depth profiles of the intrinsic region 3 in the stressed device appear comparable to those of the intrinsic region 1. The most significant discrepancies are evident in the access regions 4 and 5. As demonstrated by the LM image, there appears to be a higher degree of observable degradation in access region 5 when compared to region 4. Access region 5 has been measured as well, but the ToF-SIMS profiles could not be evaluated due to too strong degradation. The depth profiles demonstrate a substantial decline in SiN signal intensity and a strong increase in O signal in the same depth. In particular, the second SiN demonstrates a significant degree of oxidation. Furthermore, the penetration of oxygen through the epitaxial AlGaN and GaN layers in access region 4 has been observed as well.

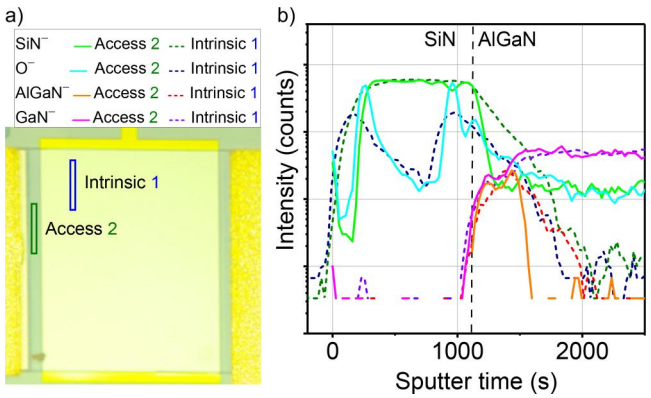

FIG. 11. (a) Locations of ToF-SIMS profiles of small areas in the intrinsic region 1 and the access region 2 of the unstressed device; (b) corresponding ToF-SIMS profiles to 1 and 2. The ToF-SIMS region of interest was $1.5 \times 28\,\mu m^2$. Besides a broader signal in the intrinsic region, there are no significant differences in signal intensities.

The presence of oxygen is predominantly observed at the interface between the first and second SiN layers. In contrast, the oxygen levels within the AlGaN and GaN layers are found to be considerably reduced. It is concluded that the principal degradation transpires within the access region, wherein the SiN is exposed to elevated levels of humidity, while the intrinsic regions benefit from the protective barrier provided by the gate metal. Overall, due to no observed changes in the intrinsic region and as suggested by the extracted activation energy, trapping could be the main contributor to the observed threshold voltage shift.

B. Investigation of morphology by scanning electron microscopy (SEM) and element distribution by element dispersive x-ray (EDX) mappings

Subsequent analysis by means of SEM and EDX is to be conducted with a focus on the access regions. It has been established that the lateral electric fields in GaN HEMTs exhibit uneven distribution, resulting in higher field intensity at the drain side as compared to the source side. This phenomenon subsequently leads to accelerated degradation in the device.[46,47] Therefore, a comparison

13 July 2026 05:29:28

© Author(s) 2026

of the source side is drawn between an unstressed [Fig. 13(a)] and a stressed [$\Delta V_{th} = 20$ V at 85% RH, Fig. 13(b)] device. This is done to potentially highlight any differences. As illustrated in Fig. 13, the initial row, designated as (**I**), exhibits the SEM images. The subsequent row, denoted as (**II**), and the final row, labelled as (**III**), present the EDX images. The former demonstrates the presence of silicon (Si) and oxygen (O) signals, while the latter indicates the presence of gallium (Ga) and nitrogen (N) signals. The investigated areas (access regions) are indicated in Fig. 8.

It has been determined that the primary degradation mechanisms are crack formation and oxidation of SiN. As is evident in the LM image, the unstressed sample does not demonstrate any significant indications of degradation. The SEM images of the stressed device on the source side (b) exhibit remarkable features. Fiber-like cracks in the SiN passivation are present along the entire device. In order to achieve a more profound comprehension of these cracks, it is necessary to refer to the EDX images. The presence of cracks is most clearly discernible in the EDX image of Si. The regions of low signal intensity exhibit a strong correlation with the corresponding areas of darkness observed in the SEM image.

The oxidation of SiN can also be evidenced in the EDX images. An accumulation of material with a flake-like shape is observed. The presence of a flake-like accumulation is accompanied by a substantial increase in the O signal and a concomitant decrease in the N signal. The Ga signal also exhibits a decrease, albeit to a lesser extent. The N signal exhibits a greater reduction in intensity compared to the Si signal, suggesting the possibility of SiN oxidation to Si oxide or a mixture, such as SiON. The same degradation behavior (i.e., cracking and oxidation) has been observed on the drain side of the device. It can be concluded from the evidence presented that there is likely to be the same degradation mechanism at play on both the source and drain sides of the DUT. Both phenomena (crack formation and oxidation) have been documented in the extant literature. Vellinga *et al.* demonstrated that the propagation speed of cracks in SiN increased in response to elevated levels of humidity.[48] Lee *et al.* demonstrated that elevated levels of humidity and temperature resulted in the oxidation of SiN, leading to an increased surface roughness and a reduction in film density.[49] The oxidation process of SiN in the presence of moisture is described in more detail in Ref. 50.

V. MODEL FOR THE HUMIDITY-INDUCED IMPACT ON V_{th}

The results of Sec. IV like oxidation of SiN ultimately modify the electrostatics of the SiN/AlGaN/GaN heterostructure. This can be formulated within a one-dimensional (1D) model of the gate stack, following the electrostatic treatment,[51] and is fully consistent with the polarization-based description of 2DEG formation.[52,53]

For a pseudomorphic SiN/AlGaN/GaN HEMT, the difference in spontaneous and piezoelectric polarization between AlGaN and GaN gives rise to a positive bound polarization charge density at the AlGaN/GaN interface and a negative bound polarization charge of similar magnitude at the AlGaN surface.[52] Without a metal gate, the positive interfacial polarization charge is partially screened by the 2DEG, while the negative surface polarization

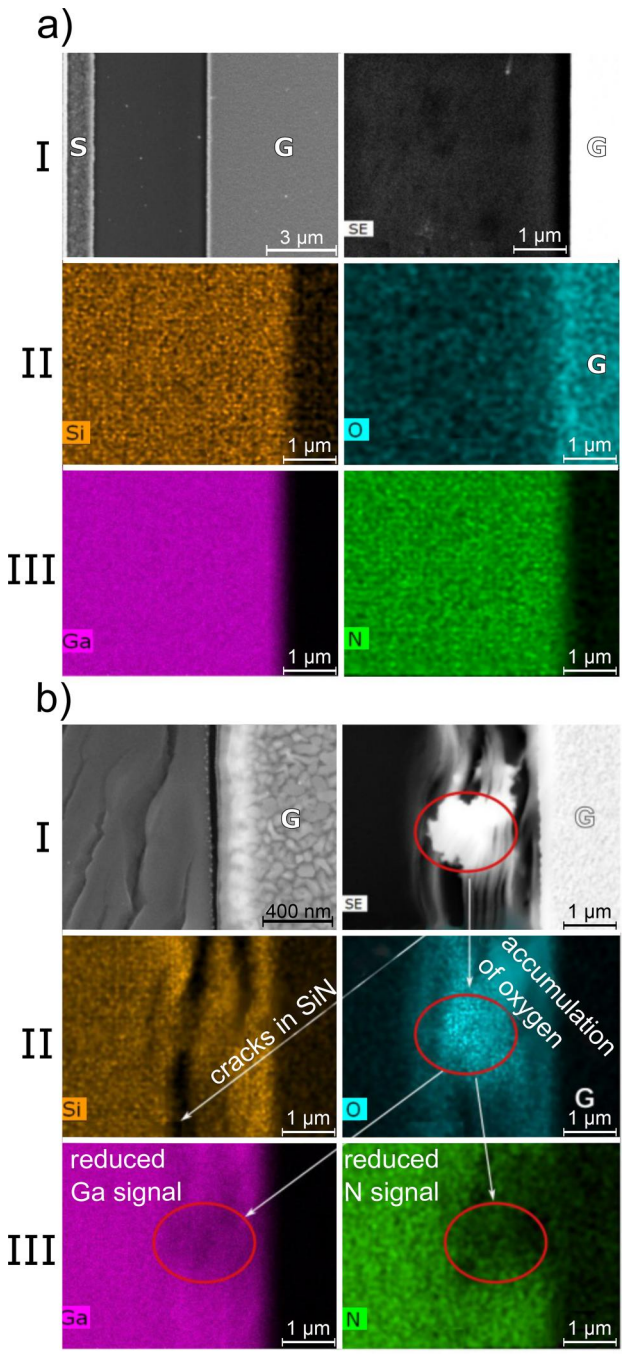

FIG. 13. A comparison of the (a) unstressed and (b) stressed devices [85% relative humidity (RH); base plate temperature $T_{bp} = 85$ °C; gate voltage $V_G = -20$ V; drain voltage $V_D = 10$ V; stress time $t_{stress} = 70$ h] on the source side is presented herein. The scanning electron microscopy (SEM) images illustrate the morphology, while the element dispersive x-ray (EDX) mappings demonstrate the element distribution. An analogous analysis for the drain side has been performed, which showed the same results. Cracks in the SiN and oxidation can be observed in the stressed device.

13 July 2026 05:29:28

© Author(s) 2026

charge is compensated by positively charged surface states or adsorbates.[53]

By including a gate and passivation, the AlGaN barrier and any dielectric layers can be treated (1D approximation) as a series capacitor between the gate metal and the 2DEG. The total sheet charge in this region adheres to Gauss's law.[51,54]

Integrating Poisson's equation from the gate metal to just inside the GaN, and grouping all contributions as sheet charges, the charge-balance condition can be written as

$$Q_G + Q_{pol} + Q_{surf} + Q_{trap} + Q_{humid} + Q_{2DEG} = 0, \quad (5)$$

where Q_G is the gate charge, Q_{pol} is the net bound polarization charge in the AlGaN/GaN system (including the surface and interface contributions), Q_{surf} accounts for the charge in "intrinsic" surface/interface states in the dry, unstressed device, Q_{trap} represents charge trapped under electrical stress in the absence of humidity, Q_{humid} is the additional fixed charge associated with humidity-related species (e.g., OH^-, O-related defects),[55] and $Q_{2DEG} = -q\,n_s$ is the charge of the 2DEG at the AlGaN/GaN interface, with n_s being the sheet density. Equation (5) shows that the vertical component of the electric displacement field is continuous across the gate stack, and that any change in one of the sheet charge contributions must be accommodated by a corresponding change in the others.[51,52]

Under the gate, the metal/SiN/AlGaN/GaN stack can be treated as an effective parallel-plate capacitor between the gate and the 2DEG, characterized by an effective capacitance per unit area C_{eff}. In a charge-control description, the channel charge density can be expressed by

$$Q_{ch} \equiv Q_{2DEG} = -qn_s \approx C_{eff}(V_G - V_{th}), \quad (6)$$

where V_G is the applied gate-source voltage and V_{th} is the threshold voltage defined as the gate bias at which the 2DEG is just depleted under the gate. Combining the charge-control relation in Eq. (6) with the charge-balance condition in Equation (5) makes explicit that both n_s and V_{th} depend on all fixed charge contributions in the barrier and at its interfaces.

The effect of humidity is introduced distinctly: Oxidation is expected to predominantly generate *negative* charge in the passivation and at the SiN/AlGaN interface (OH^-, O-related defects). In Eq. (5), this corresponds to a change $\Delta Q_{humid} < 0$. Linearizing the 1D electrostatic solution with respect to this additional charge leads to

$$\Delta n_s \approx -\frac{\Delta Q_{humid}}{q}, \quad (7)$$

i.e., a more negative Q_{humid} directly reduces the 2DEG sheet density. At the same time, the threshold voltage shifts according to

$$\Delta V_{th} \approx -\frac{\Delta Q_{humid}}{C_{eff}}, \quad (8)$$

which is the result for a change of fixed charge in a gate stack derived from Ridley's electrostatic analysis.[51] For $\Delta Q_{humid} < 0$, Eq. (8) predicts a positive shift of V_{th}, i.e., a more positive gate bias is required to induce the same 2DEG density as in the unstressed state. This model offers a possible explanation for the observed positive threshold voltage shifts.

VI. CONCLUSION

It has been shown that increasing temperature and humidity at a constant gate and drain bias is detrimental to the reliability of GaN MISHEMT TS. By comparing devices with different SiN passivation thicknesses, it has been demonstrated that thick gate passivation significantly reduces humidity-induced degradation, underlining both the strong impact of environmental conditions and the effectiveness of sufficient passivation.

Subsequent failure analysis revealed that degradation mainly occurs in the access region rather than the intrinsic region, as determined by ToF-SIMS. The findings have demonstrated that humidity plays a substantial role in the degradation process, leading to the formation of cracks and the oxidation of SiN, as confirmed by SEM/EDX. The intrinsic region beneath the gate metal is comparatively well protected.

Also, a model for the threshold voltage shifts based on the influence of humidity has been proposed.

Taken together, the C(V)-based degradation analysis, the extraction of humidity and temperature acceleration parameters within Peck's model, and the spatially resolved failure analysis provide a consistent, physically grounded picture of humidity- and temperature-induced degradation in SiN-passivated GaN MISHEMTs. Even though the TS exhibits less complicated gate geometry and a gate length that is much longer than that of conventional HEMTs, the epitaxial stack and passivation remain similar. Consequently, it can be concluded that the findings can be transferred to GaN HEMTs.

Further studies published at the IRPS 2026 will investigate the influence of the electric field experimentally and theoretically using TCAD simulations, as well as examining potential interdependencies with the stressors, humidity, and temperature.

ACKNOWLEDGMENTS

The authors gratefully acknowledge the financial support provided by the GANYDEM project.

AUTHOR DECLARATIONS

Conflict of Interest

The authors have no conflicts to disclose.

Author Contributions

Benjamin Weber: Conceptualization (lead); Data curation (lead); Formal analysis (lead); Investigation (lead); Methodology (lead); Validation (equal); Visualization (lead); Writing – original draft (lead). **Patricie Merkert:** Data curation (supporting); Funding acquisition (lead); Writing – review & editing (supporting). **Rüdiger Quay:** Funding acquisition (equal); Supervision (equal). **Michael Dammann:** Investigation (supporting); Supervision (equal); Writing – review & editing (equal). **Peter Brückner:**

13 July 2026 05:29:28

© Author(s) 2026

Resources (equal). **Patrik Straňák:** Formal analysis (supporting); Writing – review & editing (equal). **Lutz Kirste:** Resources (supporting). **Heiko Czap:** Formal analysis (supporting). **Martina Baeumler:** Formal analysis (supporting); Methodology (supporting). **Helmer Konstanzer:** Methodology (supporting); Resources (supporting). **Philipp Neininger:** Writing – review & editing (equal).

DATA AVAILABILITY

The data that support the findings of this study are available from the corresponding author upon reasonable request.

REFERENCES

[1]R. Quay, *Gallium Nitride Electronics*, 1st ed. (Springer, Berlin, Germany, 2008), pp. 8–21.
[2]C. Liu, Y. Chen, Y. Xie, H. Liu, and Z. Cai, "Electrical properties and reliability of AlGaN/GaN high electron mobility transistor under RF overdrive stress at high temperature," Micromachines **15**, 1100 (2024).
[3]Y. Wu, C.-Y. Chen, and J. A. del Alamo, "Electrical and structural degradation of GaN high electron mobility transistors under high-power and high-temperature Direct Current stress," J. Appl. Phys. **117**, 025707 (2015).
[4]J. Lundh, A. Jacobs, M. Liao, J. Spencer, G. Foster, A. Koehler, V. Odnoblyudov, M. Tadjer, K. Hobart, and T. Anderson, "High temperature operation of GaN high electron mobility transistors on large-area engineered substrates for extreme environments," in *CS MANTECH* (CS MANTECH Association, 2000).
[5]F. Gao, D. Chen, B. Lu, H. L. Tuller, C. V. Thompson, S. Keller, U. K. Mishra, and T. Palacios, "Impact of moisture and fluorocarbon passivation on the current collapse of AlGaN/GaN HEMTs," IEEE Electron. Device Lett. **33**, 1378–1380 (2012).
[6]F. Gao, S. C. Tan, J. A. del Alamo, C. V. Thompson, and T. Palacios, "Impact of water-assisted electrochemical reactions on the off-state degradation of AlGaN/GaN HEMTs," IEEE Trans. Electron Devices **61**, 437–444 (2014).
[7]M. Meneghini, C. De Santi, I. Abid, M. Buffolo, M. Cioni, R. A. Khadar, L. Nela, N. Zagni, A. Chini, F. Medjdoub, G. Meneghesso, G. Verzellesi, E. Zanoni, and E. Matioli, "GaN-based power devices: Physics, reliability, and perspectives," J. Appl. Phys. **130**, 181101 (2021).
[8]E. Zanoni, F. Rampazzo, C. De Santi, Z. Gao, C. Sharma, N. Modolo, G. Verzellesi, A. Chini, G. Meneghesso, and M. Meneghini, "Failure physics and reliability of GaN-Based HEMTs for microwave and millimeter-wave applications: A review of consolidated data and recent results," Phys. Status Solidi (a) **219**, 2100722 (2022).
[9]A. Talukder, M. R. Ifty, and A. Al Fahad, "Comprehensive review of GaN HEMTs: Architectures, recent developments, reliability concerns, challenges, and multifaceted applications," e-Prime - Adv. Electr. Eng. Electron. Energy **13**, 101059 (2025).
[10]E. Zanoni, M. Meneghini, G. Meneghesso, F. Rampazzo, D. Marcon, V. Zhan, F. Chiocchetta, A. Graff, F. Altmann, M. Simon-Najasek, and D. Poppitz, "Reliability physics of GaN HEMT microwave devices: The age of scaling," in *International Reliability Physics Symposium (IRPS) 2020* (IEEE, 2020), pp. 1–10.
[11]S. Warnock, A. Lemus, J. Joh, S. Krishnan, S. Pendharkar, and J. A. del Alamo, "Time-dependent dielectric breakdown in high-voltage GaN MIS-HEMTs: The role of temperature," IEEE Trans. Electron Dev. **64**, 3132–3138 (2017).
[12]E. S. Lee, L. Hurtado, J. Joh, S. Krishnan, S. Pendharkar, and J. A. Del Alamo, "Time-dependent dielectric breakdown under AC stress in GaN MIS-HEMTs," in *2019 IEEE International Reliability Physics Symposium (IRPS)* (IEEE, 2019), pp. 1–5.
[13]J. A. del Alamo and J. Joh, "GaN HEMT reliability," Microelectron. Reliab. **49**, 1200–1206 (2009).
[14]D. Jin, J. Joh, S. Krishnan, N. Tipirneni, S. Pendharkar, and J. A. del Alamo, "Total current collapse in high-voltage GaN MIS-HEMTs induced by Zener trapping," in *2013 IEEE International Electron Devices Meeting* (IEEE, 2013), pp. 6.2.1–6.2.4.
[15]M. Hua, C. Liu, S. Yang, S. Liu, K. Fu, Z. Dong, Y. Cai, B. Zhang, and K. J. Chen, "Characterization of leakage and reliability of SiN_x: Gate dielectric by low-pressure chemical vapor deposition for GaN-based MIS-HEMTs," IEEE Trans. Electron Devices **62**, 3215–3222 (2015).
[16]P. Neininger, M. Mikulla, P. Döring, M. Dammann, F. Thome, S. Krause, D. Schwantuschke, P. Brückner, C. Friesicke, and R. Quay, "Advances in GaN devices and circuits at higher mm-wave frequencies," e-Prime - Adv. Electr. Eng. Electron. Energy **4**, 100177 (2023).
[17]D. Schwantuschke, E. Ture, P. Brückner, P. Neininger, A. Tessmann, M. Zink, M. Kuri, D. Meder, S. Wagner, and R. Lozar, "GaN-based power amplifier MMIC and module for D-band applications," in *2023 18th European Microwave Integrated Circuits Conference (EuMIC)* (IEEE, 2023), pp. 129–132.
[18]D. Schwantuschke, B.-J. Godejohann, S. Breuer, P. Bruckner, M. Mikulla, R. Quay, and O. Ambacher, "Broadband E-band power amplifier MMIC based on an AlGaN/GaN HEMT technology with 30 dBm output power," in *2016 IEEE Compound Semiconductor Integrated Circuit Symposium (CSICS)* (IEEE, 2016), pp. 1–4.
[19]D. Schwantuschke, P. Brückner, S. Wagner, M. Dammann, M. Mikulla, and R. Quay, "Enhanced GaN HEMT technology for E-band power amplifier MMICs with 1W output power," in *2017 IEEE Asia Pacific Microwave Conference (APMC)* (IEEE, 2017), pp. 395–398.
[20]L. Guo, X. Wang, C. Wang, H. Xiao, J. Ran, L. Weijun, X. Wang, B.-Z. Wang, C. Fang, and G. Hu, "The influence of 1 nm AlN interlayer on properties of the $Al_{0.3}Ga_{0.7}N$/AlN/GaN HEMT structure," Microelectron. J. **39**, 777–781 (2008).
[21]R. S. Balmer, K. P. Hilton, K. J. Nash, M. J. Uren, D. J. Wallis, D. Lee, A. Wells, M. Missous, and T. Martin, "Analysis of thin AlN carrier exclusion layers in AlGaN/GaN microwave heterojunction field-effect transistors," Semicond. Sci. Technol. **19**, L65 (2004).
[22]N. Man Shrestha, Y. Li, and E. Y. Chang, "Simulation study on electrical characteristic of AlGaN/GaN high electron mobility transistors with AlN spacer layer," Jpn. J. Appl. Phys. **53**, 04EF08 (2014).
[23]R. Ramesh, P. Arivazhagan, K. Prabakaran, S. Sanjay, and K. Baskar, "Influence of AlN interlayer on AlGaN/GaN heterostructures grown by metal organic chemical vapour deposition," Mater. Chem. Phys. **259**, 124003 (2021).
[24]C. Liu, E. F. Chor, and L. S. Tan, "Investigations of HfO_2-AlGaN-GaN metal-oxide-semiconductor high electron mobility transistors," Appl. Phys. Lett. **88**, 173504 (2006).
[25]M. Fagerlind, F. Allerstam, E. Sveinbjörnsson, N. Rorsman, A. Kakanakova-Georgieva, A. Lundskog, U. Forsberg, and E. Janzén, "Investigation of the interface between silicon nitride passivations and AlGaN/AlN/GaN heterostructures by C(V) characterization of metal-insulator-semiconductor-heterostructure capacitors," J. Appl. Phys. **108**, 014508 (2010).
[26]P. D. Ye, B. Yang, K. K. Ng, J. Bude, G. D. Wilk, S. Halder, and J. C. M. Hwang, "GaN metal-oxide-semiconductor high-electron-mobility-transistor with atomic layer deposited Al_2O_3 as gate dielectric," Appl. Phys. Lett. **86**, 063501 (2005).
[27]B. M. Paine, S. R. Polmanter, V. T. Ng, N. T. Kubota, and C. R. Ignacio, "Lifetesting GaN HEMTs with multiple degradation mechanisms," IEEE Trans. Device Mater. Reliab. **15**, 486–494 (2015).
[28]M. Meneghini, I. Rossetto, D. Bisi, M. Ruzzarin, M. Van Hove, S. Stoffels, T.-L. Wu, D. Marcon, S. Decoutere, G. Meneghesso, and E. Zanoni, "Negative bias-induced threshold voltage instability in GaN-on-Si power HEMTs," IEEE Electron. Device Lett. **37**, 474–477 (2016).
[29]Y. Kurachi, H. Yamamoto, Y. Nose, S. Shimizu, Y. Tateno, T. Yonemura, and M. Furukawa, "Failure mode analysis of GaN-HEMT under high temperature operation," in *2018 IEEE International Reliability Physics Symposium (IRPS)* (IEEE, 2018) pp. P–WB.3–1–P–WB.3–4.
[30]J. A. Rodriguez, T. Tsoi, D. Graves, and S. B. Bayne, "Evaluation of GaN HEMTs in H^3TRB reliability testing," Electronics **11**, 1532 (2022).

13 July 2026 05:29:28

© Author(s) 2026

[31]S. Kunwar, C. B. Somodi, R. A. Lalk, B. X. Rutherford, Z. Corey, P. Roy, D. Zhang, M. Hellenbrand, M. Xiao, J. L. MacManus-Driscoll, Q. Jia, H. Wang, J. Joshua Yang, W. Nie, and A. Chen, "Protons: Critical species for resistive switching in interface-type memristors", Adv. Electron. Mater. **9**, 2200816 (2022).
[32]G. Greco, P. Fiorenza, F. Giannazzo, C. Bongiorno, M. Moschetti, C. Bottari, M. S. Alessandrino, F. Iucolano, and F. Roccaforte, "Threshold voltage instability by charge trapping effects in the gate region of p-GaN HEMTs," Appl. Phys. Lett. **121**, 233506 (2022).
[33]A. Brunko, M. Gloth, and N. Kaminski, "Humidity capability of enhancement mode GaN high electron mobility transistors," in *2021 IEEE 8th Workshop on Wide Bandgap Power Devices and Applications (WiPDA)* (IEEE, 2021), pp. 242–245.
[34]J. Jormanainen, E. Mengotti, T. Batista Soeiro, E. Bianda, D. Baumann, T. Friedli, A. Heinemann, A. Vulli, and J. Ingman, "High humidity, high temperature and high voltage reverse bias—a relevant test for industrial applications," in *PCIM Europe 2018* (VDE Verlag GmbH, 2018), pp. 1–7.
[35]T. Hisaka, Y. Aihara, Y. Nogami, H. Sasaki, Y. Uehara, N. Yoshida, and K. Hayashi, "Degradation mechanisms of GaAs PHEMTs in high humidity conditions," Microelectron. Reliab. **45**, 1894–1900 (2005).
[36]S. Zhou, "Experimental investigation on the performance degradations of the GaN class-F power amplifier under humidity conditions," Semicond. Sci. Technol. **36**, 035025 (2021).
[37]C.-L. Huang, S. Grot, G. Gildenblat, and V. Bolkhovsky, "Charge trapping and dielectric breakdown in MOS devices in 77–400 K temperature range," Solid-State Electron. **32**, 767–775 (1989).
[38]M. Meneghini, A. Tajalli, P. Moens, A. Banerjee, E. Zanoni, and G. Meneghesso, "Trapping phenomena and degradation mechanisms in GaN-based power HEMTs," Mater. Sci. Semicond. Process. **78**, 118–126 (2018).
[39]D. Marcon, T. Kauerauf, F. Medjdoub, J. Das, M. Van Hove, P. Srivastava, K. Cheng, M. Leys, R. Mertens, S. Decoutere, G. Meneghesso, E. Zanoni, and G. Borghs, "A comprehensive reliability investigation of the voltage-, temperature- and device geometry-dependence of the gate degradation on state-of-the-art gan-on-si hemts," in *2010 International Electron Devices Meeting* (IEEE, 2010), pp. 20.3.1–20.3.4.
[40]H. Sun, M. Montes Bajo, M. Uren, and M. Kuball, "Implications of gate-edge electric field in AlGaN/GaN high electron mobility transistors during off-state degradation," Microelectron. Reliab. **54**, 2650–2655 (2014).
[41]E. H. Wong, J. Cook, M. Dreno, D.-L. Chen, and Y.-S. Lai, "Characterising arrhenius moisture diffusivity constants using non-isothermal sorption," Microelectron. Reliab. **55**, 2331–2335 (2015).
[42]R. Quay, C. Moglestue, V. Palankovski, and S. Selberherr, "A temperature dependent model for the saturation velocity in semiconductor materials," Mater. Sci. Semicond. Process. **3**, 149–155 (2000).
[43]L. Zhou, Z. San, and J.-F. Mao, "Electro-thermal-stress analysis of AlGaN/GaN HEMTs breakdown under intentional EMI," in *2016 IEEE International Symposium on Radio-Frequency Integration Technology (RFIT)* (IEEE, 2016), pp. 1–3.
[44]D. S. Peck, "Comprehensive model for humidity testing correlation," in *24th International Reliability Physics Symposium* (IEEE, 1986), pp. 44–50.
[45]D. S. McPhail, E. A. Clark, J. B. Clegg, M. G. Dowsett, J. P. Gold, G. D. T. Spiller, and D. Sykes, "The depth resolution of secondary ion mass spectrometers: A critical evaluation," Scanning Microsc. **2**, 3 (1988).
[46]S. Bordoloi, A. Ray, P. Barman, and G. Trivedi, "Investigation of electric field profile and associated parameters with embedded metal layer in field plate AlGaN/GaN HEMTs," J. Phys.: Conf. Ser. **2236**, 012005 (2022).
[47]V. G. Tikhomirov, A. Gudkov, V. Petrov, S. Agasieva, A. Zybin, V. Yankevich, and A. Evseenkov, "Simulation of electric field distribution in GaN HEMTs for the onset of structure degradation," in *2017 11th International Workshop on the Electromagnetic Compatibility of Integrated Circuits (EMCCompo)* (IEEE, 2017), pp. 115–118.
[48]W. P. Vellinga, J. T. M. De Hosson, and P. C. P. Bouten, "Effect of relative humidity on crack propagation in barrier films for flexible electronics," J. Appl. Phys. **112**, 083520 (2012).
[49]W. J. Lee, T.-Y. Cho, S.-H. Choa, and S.-K. Cho, "Environmental reliability and moisture barrier properties of silicon nitride and silicon oxide films using roll-to-roll plasma enhanced chemical vapor deposition," Thin Solid Films **720**, 138524 (2021).
[50]T. Oku, M. Okumura, M. Totsuka, T. Shiga, and M. Takemi, "Moisture resistance of insulating films for compound semiconductor devices," in *CS MANTECH 2014-2014 International Conference on Compound Semiconductor Manufacturing Technology* (CS MANTECH Association, 2014), pp. 179–182.
[51]B. K. Ridley, "Polarization-induced electron populations," Appl. Phys. Lett. **77**, 990–992 (2000).
[52]O. Ambacher, J. Smart, J. R. Shealy, N. G. Weimann, K. Chu, M. Murphy, W. J. Schaff, L. F. Eastman, R. Dimitrov, L. Wittmer, M. Stutzmann, W. Rieger, and J. Hilsenbeck, "Two-dimensional electron gases induced by spontaneous and piezoelectric polarization charges in N- and Ga-face AlGaN/GaN heterostructures," J. Appl. Phys. **85**, 3222–3233 (1999).
[53]J. P. Ibbetson, P. T. Fini, K. D. Ness, S. P. DenBaars, J. S. Speck, and U. K. Mishra, "Polarization effects, surface states, and the source of electrons in AlGan/GaN heterostructure field effect transistors," Appl. Phys. Lett. **77**, 250–252 (2000).
[54]S. Sze and K. Ng, *Physics of Semiconductor Devices*, 3rd ed. (John Wiley & Sons, Inc., Hoboken, NJ, 2006), pp. 1–815.
[55]L. L. Chua, J. Zaumseil, J.-F. Chang, E. Ou, P. Ho, H. Sirringhaus, and R. Friend, "General observation of *n*-type field-effect behaviour in organic semiconductors," Nature **434**, 194–199 (2005).

13 July 2026 05:29:28

© Author(s) 2026